ARTICLE

doi:10.1038/nature11526

A neural circuit for spatial summation in visual cortex

Hillel Adesnik[1]†, William Bruns[1], Hiroki Taniguchi[2], Z. Josh Huang[2] & Massimo Scanziani[1]

The response of cortical neurons to a sensory stimulus is modulated by the context. In the visual cortex, for example, stimulation of a pyramidal cell's receptive-field surround can attenuate the cell's response to a stimulus in the centre of its receptive field, a phenomenon called surround suppression. Whether cortical circuits contribute to surround suppression or whether the phenomenon is entirely relayed from earlier stages of visual processing is debated. Here we show that, in contrast to pyramidal cells, the response of somatostatin-expressing inhibitory neurons (SOMs) in the superficial layers of the mouse visual cortex increases with stimulation of the receptive-field surround. This difference results from the preferential excitation of SOMs by horizontal cortical axons. By perturbing the activity of SOMs, we show that these neurons contribute to pyramidal cells' surround suppression. These results establish a cortical circuit for surround suppression and attribute a particular function to a genetically defined type of inhibitory neuron.

Visual stimuli located outside of the classical receptive field of a neuron in visual cortex are unable to elicit spiking, but they may modulate the neuron's response to stimuli located in its receptive field[1–3]. Surround suppression, a basic operation in visual processing, is a classical example of this type of modulation[4–9] and can be easily observed when monitoring the firing of a neuron to a stimulus of increasing size centred on its receptive field (that is, the size tuning of the neuron): the neuron's initial increase in firing is followed by a decrease in firing as the stimulus becomes progressively larger. This form of suppression has been suggested to contribute to a number of perceptual effects like pop-out, curvature detection and orientation discrimination[8,10–12]. Importantly surround suppression is not only observed in the cortex but is already present at earlier stages along the visual hierarchy, namely in the retina[13–15] and the thalamus[14,16–18]. Thus, although it is likely that at least part of the suppressive surround observed in the cortex is relayed from earlier stages of visual processing[19], some experimental observations and theoretical models suggest that the cortex is itself capable of contributing to surround suppression[20–22]. Here we reveal the identity and describe the mechanism of a cortical circuit that directly contributes to surround suppression in the superficial layers of the primary visual cortex.

Neuron-type-specific spatial summation

We determined the tuning to the size of a visual stimulus for neurons in the superficial layers of the primary visual cortex (V1; depth ~100–350 μm, corresponding approximately to layers 2 and 3 (layer 2/3)) of mice. Experiments were performed in awake, running animals, as size tuning was affected by anaesthesia (Supplementary Fig. 1). Mice were head fixed but otherwise unrestrained and free to run on a passive circular treadmill. To reduce variability due to differences in behavioural state, all data presented here were recorded during running events (see Supplementary Methods).Visual stimuli were composed of circular patches of drifting gratings at maximal contrast, presented in 6 or 7 different sizes (from 8 to 97 degrees in diameter, Fig. 1a). The size-tuning curve of isolated units[23] ($n = 53$; Supplementary Fig. 2), that is, the neuronal firing rate as a function of stimulus size, peaked at 22 ± 2 degrees (preferred size; ± s.e.m.) and progressively decreased with larger stimuli (Fig. 1a, d), revealing marked surround suppression[24]. The mean firing rates (± s.e.m.) were 0.47 ± 0.11 Hz (at the baseline (FR_{BL})); 3.0 ± 1.0 Hz in response to the smallest stimulus (FR_{SS}); 3.1 ± 0.3 Hz in response to the preferred stimulus (FR_{PS}); and 1.0 ± 0.2 Hz in response to the largest stimulus (FR_{LS}). The stimulus modulation index (SMI, computed as $(FR_{PS} - FR_{BL})/FR_{PS}$) was 0.87 ± 0.03. The suppression index, that is, the difference between the peak response and the response to the largest stimulus, divided by the baseline subtracted peak response ($(FR_{PS} - FR_{LS})/(FR_{PS} - FR_{BL})$; Fig. 1a) averaged 0.9 ± 0.1 ($n = 53$; the suppression index was statistically significant in 33 out of 53 units (permutation test); Fig. 1d), indicating substantial suppression in response to large stimuli. Infrequent eye movements occurring during running had little effect on the size-tuning curve (Supplementary Fig. 3).

If cortical circuits contribute to surround suppression they may involve the suppressive action of cortical inhibitory neurons. An inhibitory neuron lacking surround suppression and whose response increases with stimulus size would be a good candidate. In cat visual cortex, for example, fast spiking inhibitory neurons respond with higher firing rates to large stimuli than to small visual stimuli[22]. We carried out targeted loose-patch recordings from inhibitory neurons in layer 2/3 of V1 in awake, running mice, using two-photon laser scanning microscopy[25] (Fig. 1b, c). Parvalbumin-expressing neurons (PVs)[26], a large class of cortical inhibitory neurons, were visualized in layer 2/3 by crossing a PV–Cre mouse line with a tdTomato-reporter line. The size-tuning curve of PVs peaked at 57 ± 8 degrees ($n = 11$) and showed marked surround suppression with larger stimuli (suppression index, 0.46 ± 0.12, $n = 11$; suppression index statistically significant in 6 out of 11 cells, permutation test (Fig. 1b, e); FR_{BL}, 9 ± 2 Hz; FR_{SS}, 27 ± 7 Hz; FR_{PS}, 45 ± 11 Hz; FR_{LS}, 26 ± 8 Hz; SMI, 0.74 ± 0.07; recorded PVs showed their characteristic 'thin' spike shapes (Supplementary Fig. 2), confirming the accuracy of our targeting strategy[23,27]). In contrast to PVs, SOMs, another large class of cortical inhibitory neurons[26] (visualized by crossing a SOM–Cre line with a tdTomato-reporter line[28]), completely lacked surround suppression (suppression index, 0.09 ± 0.06; $n = 8$; suppression index statistically

[1]Howard Hughes Medical Institute, Center for Neural Circuits and Behavior, Neurobiology Section and Department of Neuroscience, University of California San Diego, La Jolla, California 92093-0634, USA. [2]Cold Spring Harbor Laboratory, 1 Bungtown Road, Cold Spring Harbor, New York 11724, USA. †Present address: Department of Molecular and Cell Biology and the Helen Wills Neuroscience Institute, University of California, Berkeley 94720, USA.

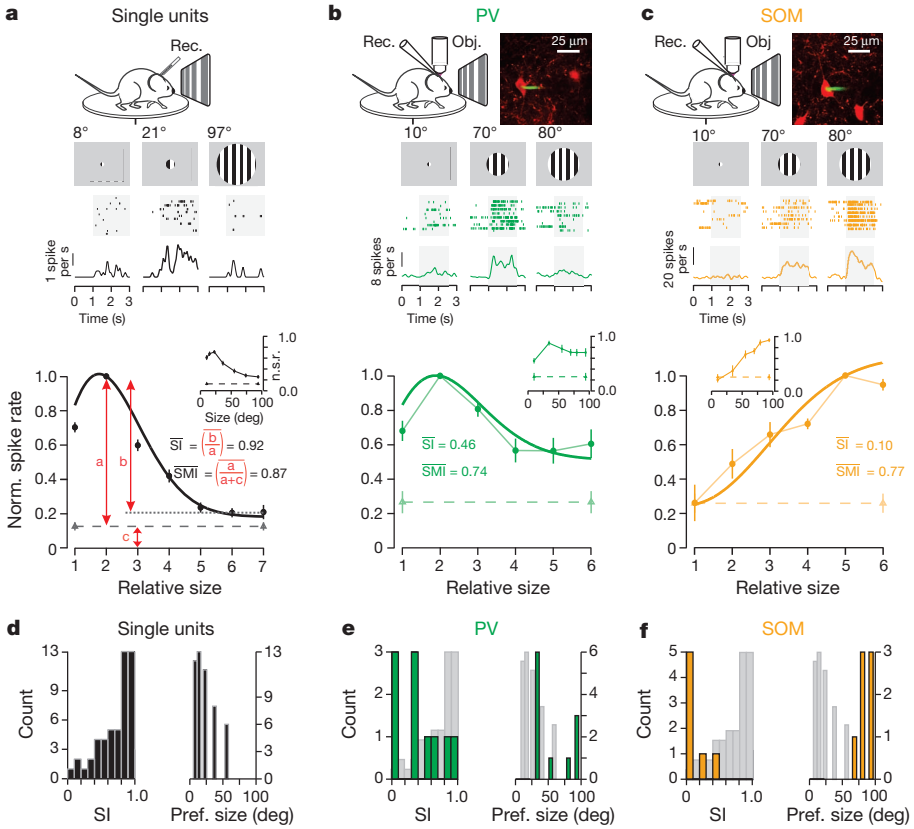

Figure 1 | Differences in spatial summation between three types of neurons in the visual cortex. **a**, Top, schematic of the experimental setup. Centre, response of example unit to visual stimuli of three different sizes (a raster plot and a peristimulus time histogram (PSTH) are shown). Shaded area behind the raster plot represents the period of stimulus presentation. Bottom, average size-tuning curve of 53 peak-aligned and normalized single units (6 animals, 11 recording sessions). Grey triangles with dashed lines, baseline firing rate. Inset, average of the normalized but not peak-aligned 53 size-tuning curves. SI, suppression index; SMI, stimulus modulation index. **b**, Top left, schematic of the experimental setup. Top right, tdTomato-expressing PV (red) with attached Alexafluor-488-filled recording pipette (green). Center, response of PV to visual stimuli of three different sizes (a raster plot and a PSTH are shown). Bottom, average size-tuning curve ($n = 11$ peak-aligned and normalized size-tuning curves; 3 animals). Inset, average of the normalized but not peak-aligned 11 size-tuning curves. Obj., microscope objective. **c**, As in **b** but for SOMs ($n = 7$; 4 animals). **d**–**f**, Distribution of SIs (left panels) and of preferred stimulus sizes (right panels) for single units (**d**), PVs (**e**) and SOMs (**f**). The SOM and PV data are superimposed onto the single-unit data (grey, from **e**) for comparisons. All error bars are s.e.m.

significant in 0 out of 8 cells; permutation test; significantly different from PVs; $P < 0.03$, rank sum test; Fig. 1f). The size-tuning curve of these neurons showed a monotonic increase or saturation in firing rate with stimulus size (Fig. 1c, f). Although the smallest stimuli were relatively inefficient in driving SOMs (FR_{BL}, 7 ± 2 Hz; FR_{SS}, 5 ± 2 Hz), they robustly responded to large stimuli (FR_{PS}, 26 ± 2 Hz; preferred size, 86 ± 3 degrees, different from PV, $P < 0.015$, rank sum test; SMI, 0.75 ± 0.05). These data demonstrate that in V1, spatial summation can be very different between genetically distinct types of neurons. Furthermore, these data suggest that SOMs are potential candidates in the generation of cortical surround suppression.

Excitation of SOMs by horizontal axons

In response to the observations above, we examined two fundamental issues: first, what cortical circuits enable SOMs, in contrast to other cortical neurons, to be facilitated rather than suppressed by large stimuli; and second, whether SOMs contribute to size tuning in V1.

The two predominant excitatory inputs to layer 2/3 are vertically ascending axons from layer 4 and horizontally projecting axons from layer 2/3. To examine whether SOMs are equally excited by these two inputs, we recorded from layer 2/3 pyramidal cells, SOMs and PVs in coronal slices of V1 and selectively photo-activated (light ramp of 2 s duration; 480 nm light) layer 4 excitatory cells that conditionally expressed channelrhodopsin 2 (ChR2; Supplementary Fig. 4)[29]. Layer 4 photostimulation generated excitatory charges in SOMs that were only $17 \pm 5\%$ ($\pm$ s.e.m.; $n = 8$) of those in simultaneously recorded pyramidal cells (Fig. 2a); in contrast, excitatory charges generated in PVs were $250 \pm 39\%$ ($n = 8$) of those generated in simultaneously recorded pyramidal cells (Fig. 2b). These results were corroborated through ChR2-assisted circuit mapping[30] (Supplementary Fig. 5). Thus, ascending layer 4 axons provide little excitation to SOMs. Notably, photostimulation of layer 2/3 pyramidal cells (2 s light ramp duration) that selectively expressed ChR2 (see methods[31]) produced substantial excitation of layer 2/3 SOMs (Fig. 2d): the excitation that SOMs received was in fact significantly larger than that received by simultaneously recorded pyramidal cells ($241 \pm 85\%$, $n = 7$, $P < 0.05$; Fig. 2e; we selectively recorded from pyramidal cells that did not express ChR2 in order to avoid contamination with photocurrents[31]). Furthermore, although photostimulation of horizontal layer 2/3 projections was accompanied by strong disynaptic inhibition in pyramidal cells, very little inhibition was recorded in SOMs (Fig. 2e; the ratio of excitation to the sum of excitation and inhibition (E/(E + I)) was 0.11 ± 0.01 ($n = 10$) in pyramidal cells versus 0.59 ± 0.06 ($n = 11$) in SOMs; $P < 0.05$, Fig. 2f). These results show that although layer 2/3 pyramidal cells and PVs receive substantial excitatory drive from ascending layer 4 axons, the main excitation to layer 2/3 SOMs are horizontal axons of layer 2/3.

Size-dependent excitation of SOMs

To ascertain whether these horizontal axons are indeed responsible for the size-dependent recruitment of SOMs, we took advantage of the retinotopic organization of V1 (ref. 32); we reasoned that because

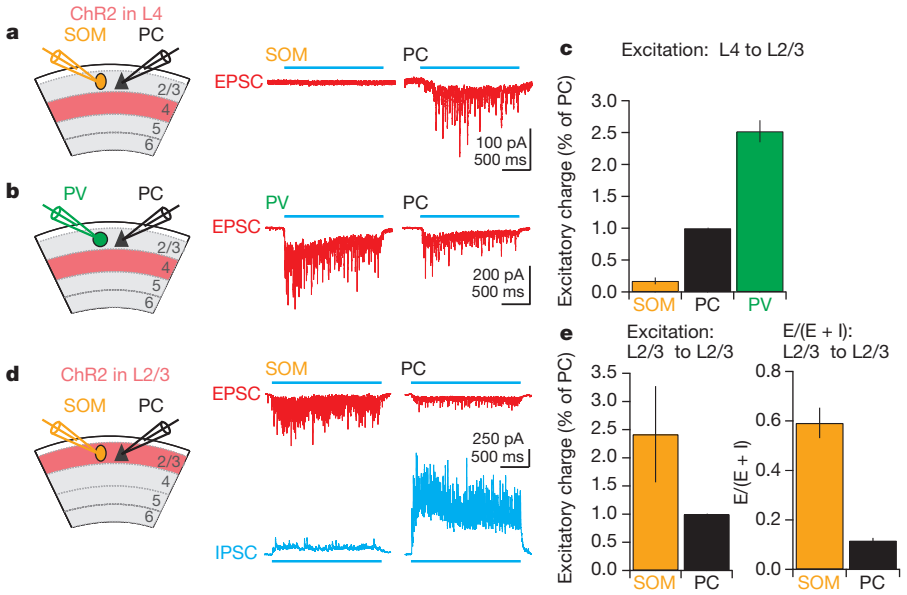

Figure 2 | SOMs are selectively excited by horizontal cortical projections. **a**, Left, schematic of the experimental setup. ChR2 is expressed selectively in layer 4 (L4) excitatory neurons. Recording electrodes in layer 2/3 (L2/3) target a SOM and a pyramidal cell (PC). Right, excitatory currents simultaneously recorded in a SOM and a PC in response to photostimulation of layer 4 with a ramp of blue light (horizontal blue line). EPSC, excitatory postsynaptic current. **b**, Left, schematic of the experimental setup. As in **a** but whole-cell recording electrodes in layer 2/3 target a PV and a PC. Right, excitatory currents simultaneously recorded in a PV and a PC in response to photostimulation of layer 4 as in **a**. **c**, Summary statistics of the excitatory charge (as a fraction of that simultaneously recorded in the PC) recorded in SOMs ($n = 8$) and PVs ($n = 8$); $P < 0.05$. **d**, Left, schematic of the experimental setup. As in **a** except ChR2 is expressed selectively in PCs of layer 2/3. Right, excitatory currents (red, top traces) and inhibitory currents (bottom, blue traces) simultaneously recorded in a SOM and a PC in response to photostimulation of layer 2/3 with a ramp of blue light. IPSC, inhibitory postsynaptic current. **e**, Left, summary statistics of excitatory charge (as a fraction of that simultaneously recorded in the PC) recorded in SOMs compared to that recorded in layer 2/3 PCs ($n = 7$, $P < 0.05$). Right, ratio of excitation to inhibition (expressed as E/E + I) recorded in SOMs and PCs ($n = 10$, $P < 0.05$). All error bars are s.e.m.

progressively larger visual stimuli presented *in vivo* will result in a progressively larger visually activated area in V1, we could approximate this expansion of activity by directly photostimulating progressively larger areas of V1. We carried out loose-patch recordings from SOMs in coronal slices of V1 expressing ChR2 in layer 2/3 pyramidal cells (Fig. 3a). The firing rate of SOMs increased as a function of the size of the light spot (180 to 900 μm), similar to their increase in firing rate *in vivo* with increasing visual stimulus size (Fig. 3a, b). Consistent with the increase in firing rate, the synaptic excitation received by SOMs increased with increasing light spot size (Fig. 3a, b). If SOM dendrites were to span areas similar to the largest light-spot diameter, the progressive increase in firing rate with spot size might simply result from the direct photostimulation of synapses on the dendritic arborization of the recorded SOM. However, this was not the case because even the smallest light spot used (180 μm diameter), generating only approximately 25% of the maximal firing rate, covered more than 95% of the entire SOM dendritic arborization (Fig. 3b, see Supplementary Methods). Thus, the increase in SOM firing rate with spot size results from the recruitment of progressively more distant L2/3 pyramidal cells (Fig. 3b, see methods). Furthermore, cutting horizontal axons with two vertical cuts through layer 2/3 on each side of the recorded SOMs (320 ± 25 μm (± s.e.m.) between cuts, centred on the cell, $n = 10$; note that the distance between the cuts is larger than the horizontal dendritic extent of SOMs) prevented the increase in firing rate with stimuli larger than the distance between the two cuts (Supplementary Fig. 6). Thus, by using horizontal layer 2/3 projections as their main excitatory drive, SOMs are recruited as a function of the activated V1 area; that is, they sum activity in visual space.

Is the size-dependent recruitment of SOMs a mechanism that could contribute to the suppression of pyramidal-cell firing to large stimuli? We recorded from pyramidal cells in coronal slices of V1 conditionally expressing ChR2 in layer 2/3 (again, we selectively recorded from pyramidal cells that did not express ChR2). The firing rate of pyramidal cells was set to approximately 10 Hz by direct-current injection (Fig. 3c). A small light spot centred around the recorded pyramidal cell reduced the firing rate, and this suppression became progressively more pronounced as a larger area of layer 2/3 was activated by increasing the size of the light spot (Fig. 3c). Consistent with the progressive suppression in firing rate, the inhibition received by pyramidal cells increased with increasing light-spot size (Fig. 3c,d). Finally, to establish that the inhibition generated in pyramidal cells after photo-activation of layer 2/3 (ref. 31) was due to the recruitment of SOMs[33] and not any other interneuron type, we optogenetically silenced SOMs (see Methods) while monitoring the inhibition in pyramidal cells during photoactivation of layer 2/3 (Fig. 3e). Photostimulation of layer 2/3 to activate pyramidal cells generated strong firing in SOMs and large inhibitory currents in simultaneously recorded pyramidal cells, consistent with the results reported above (Fig. 3e). Notably, concomitant optogenetic silencing of SOMs (100% reduction of firing; $n = 6$) strongly reduced the inhibitory currents in pyramidal cells (80 ± 4% reduction (± s.e.m.); $n = 8$, $P < 0.05$, Fig. 3e, f).

Thus, the stimulus-size-dependent recruitment of SOMs generates strong inhibition in layer 2/3 pyramidal cells and efficiently suppresses their firing rate (Fig. 3g).

SOMs contribute to surround suppression

These data provide a plausible mechanism by which SOMs could contribute to surround suppression of layer 2/3 pyramidal cells *in vivo*. Furthermore, under anaesthesia, a situation in which surround suppression is compromised (see above and Supplementary Fig. 1), the firing rate of SOMs was reduced tenfold (from 26 ± 2 Hz, $n = 8$ to 2.7 ± 0.4 Hz, $n = 10$), much more than that of single units or PVs (Supplementary Fig. 1). This is consistent with a possible contribution of SOMs to surround suppression. To test directly for the involvement of SOMs in surround suppression, we conditionally expressed the light-sensitive hyperpolarizing opsin archaerhodopsin (Arch)[34] in V1 using viral injection of a flexed Arch vector[35]into SOM-Cre mice (71 ± 2% of cells infected (± s.e.m.), $n = 4$ animals; Fig. 4b and Methods). Illumination of the cortical surface efficiently reduced the

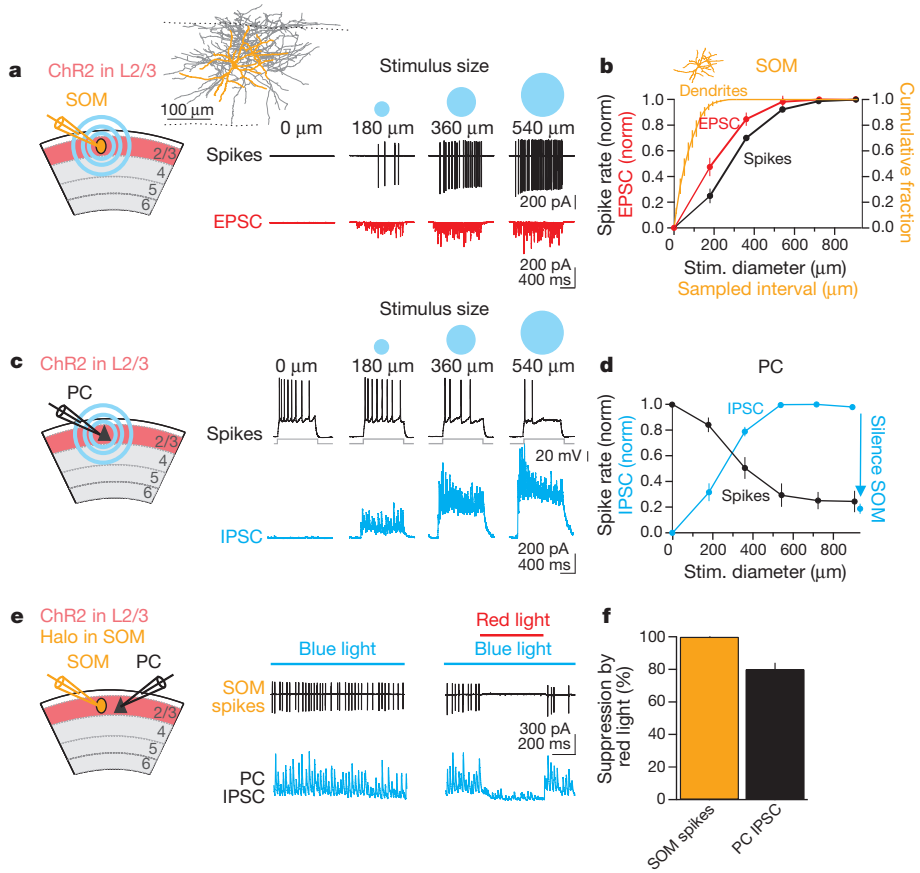

Figure 3 | Suppression of pyramidal cells by SOMs as a function of the activated layer 2/3 area. **a**, Left, schematic of the experimental setup. ChR2 is expressed in a fraction of PCs in layer 2/3. Inset, anatomical reconstruction of a biocytin-filled layer 2/3 SOM (dendrites, orange; axon, grey; top dotted line, border with layer 1; bottom dotted line, border with layer 4). Right, action potentials (black traces, top) recorded in the cell-attached mode in a SOM in response to light-spot sizes of increasing diameter. Bottom, excitatory currents (red traces) recorded subsequently in the whole-cell voltage-clamp configuration in the same SOM neuron in response to the same photo-stimuli. EPSC, excitatory postsynaptic current. **b**, Summary graph for the spiking (black; $n = 14$) and excitatory charge (red; $n = 6$) of SOMs in response to light spots of five different diameters. Orange, summary statistics of the cumulative fraction of SOM dendritic arbor length within a sampled horizontal interval centred on the SOM cell body ($n = 6$). Inset, dendrites of the SOM illustrated in **a** but scaled to x axis. **c**, Left, schematic of the experimental setup. As in **a** but recording from PC. Right, spiking of PC recorded in current-clamp mode (black traces) in response to depolarizing current steps while layer 2/3 is photo-stimulated with increasingly large blue light spots (top), and inhibitory currents recorded in a PC to the same light stimuli (bottom). IPSC, inhibitory postsynaptic current. **d**, Summary graph of the suppression of firing of PCs (black, $n = 7$) and intracellularly recorded inhibitory charge (blue, $n = 6$) to light spots of five different diameters. Photo-hyperpolarizing SOMs (blue arrow; see **e**) reduce inhibitory charge in PCs. **e**, Schematic of the experimental setup. ChR2 is expressed in a fraction of layer 2/3 PCs and halorhodopsin (halo) is conditionally expressed in SOMs. Recording electrodes target a SOM and a PC. Full-field blue light activates layer 2/3 PCs, whereas red light suppress SOMs. Traces, spikes (black traces, top) recorded in the cell-attached mode in a SOM and inhibitory currents (blue traces, bottom) simultaneously recorded in a voltage-clamped PC in response to blue light photo-stimulation (blue bar) of layer 2/3. Simultaneous illumination with red light (red bar, right panel) to photo-hyperpolarize SOMs abolishes SOM firing and reduces inhibitory currents in the PC (see also blue arrow in **d**). **f**, Summary graph for halorhodopsin-mediated reduction of SOM firing ($n = 6$) and concomitant reduction in inhibitory charge in layer 2/3 PCs ($n = 8$).

visually evoked activity of Arch-expressing layer 2/3 SOMs (80 ± 1% suppression, $n = 4$, $P < 0.05$; Supplementary Fig. 7). To determine the impact of SOMs on size tuning in layer 2/3, we performed extracellular recordings as described above and alternated control trials (visual stimulus only) with trials in which SOMs were photo-hyperpolarized (Fig. 4). Photo-hyperpolarization of SOMs significantly reduced surround suppression of layer 2/3 neurons by 30 ± 10% (± s.e.m.; $n = 28$, $P < 0.00022$, paired signed rank test, Fig. 4c–e; photo-hyperpolarization of SOMs had no significant effect on baseline firing rates, −9 ± 17% (± s.e.m.), $n = 13$, $P > 0.18$). Nearly all units (25 out of 28) showed a decrease in the suppression index (Fig. 4e), and in 10 out of 25 units the decrease was individually significant ($P < 0.05$ permutation test). The reduction of the suppression index was a result of SOM photo-hyperpolarization facilitating the response to large visual stimuli more than to small visual stimuli: the response ratio (the ratio of the firing rate in the illumination condition divided by firing rate in the control condition) increased with the size of the stimulus (Fig. 4f). Although the response to stimuli smaller or equal to the preferred size was not facilitated (−7 ± 7% (± s.e.m.), $P > 0.45$, paired signed rank test, $n = 28$; $FR_{PS,\ CTRL} = 4.9 \pm 1.5$ Hz, $FR_{PS,\ LED} = 4.6 \pm 1.9$ Hz, $P > 0.63$, paired signed rank test), the response to the stimuli larger than the preferred size was facilitated by 74 ± 19% ($P < 0.0011$, paired signed rank test, $n = 28$; Fig. 4f). This lack of facilitation of responses to smaller visual stimuli was not due to saturation (that is, a ceiling effect). In fact, firing rates to stimuli smaller or equal to the preferred one were consistently facilitated less than similar firing rates elicited by stimuli larger than the preferred one (Supplementary Fig. 8). The stronger impact of SOM photo-hyperpolarization on cortical responses to large stimuli is thus consistent with the preferential activation of SOMs by large stimuli (Fig. 1c). Hence, by inhibiting layer 2/3 neurons as a function of stimulus size, SOMs generate an inhibitory surround (Fig. 4g).

Discussion

This study describes a cortical circuit that significantly contributes to surround suppression of layer 2/3 cells, and identifies a specific type of

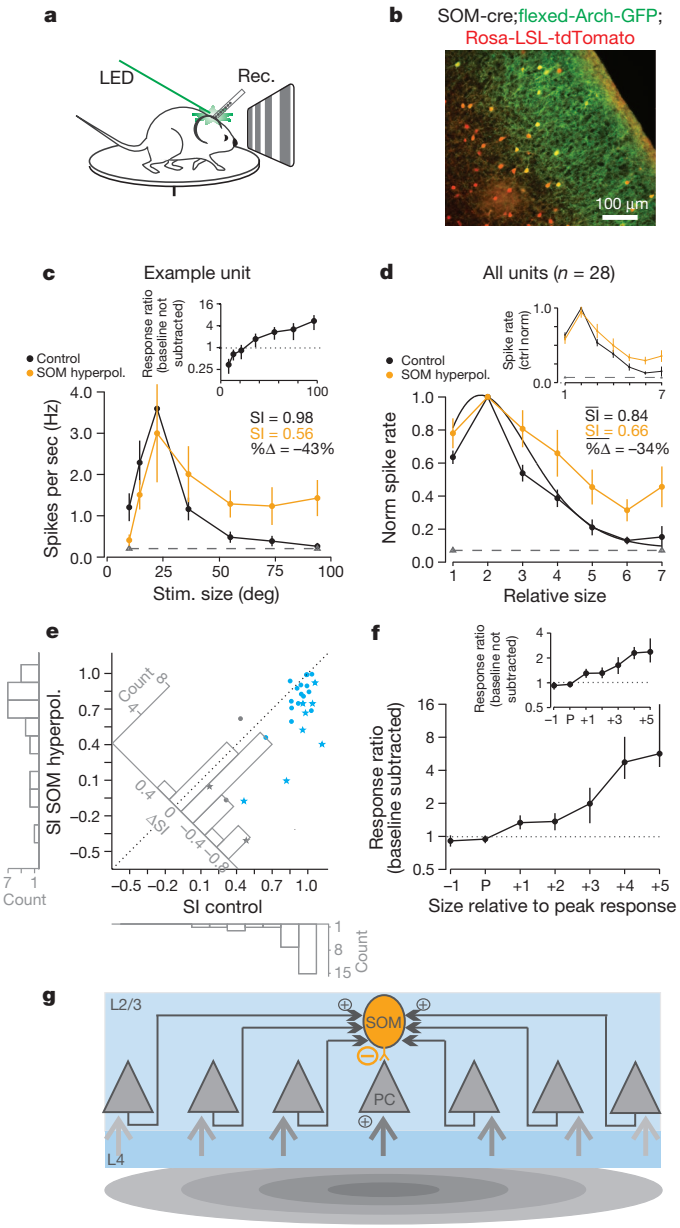

Figure 4 | SOMs contribute to size tuning of layer 2/3 pyramidal cells. **a**, Schematic of the experimental setup. **b**, Section of the visual cortex of a SOM-CRE;Rosa-LSL-tdTomato mouse injected with AAV-flexed-Arch-GFP. All SOM-CRE cells express tdTomato (red) and infected neurons also express Arch-GFP (green). **c**, Size tuning of an isolated unit in control conditions and during photo-hyperpolarization of SOMs. Dashed grey line, baseline firing rate. Inset, response ratio for this example unit. All error bars are s.e.m. **d**, Average peak-aligned and scaled size-tuning curves for 28 isolated single units (3 animals, 7 recording sessions). Black, control conditions; orange, SOM hyperpolarization. Inset, average peak-aligned and control-normalized size-tuning curve in the SOM-hyperpolarization condition. Note the lack of facilitation at the preferred or smaller size. All error bars are s.e.m. **e**, Scatter plot showing SI under control conditions (x axis) plotted against SI under SOM hyperpolarization (y axis) for each of the 28 units. Blue data points are units that are size tuned at baseline ($n = 24$, SI > 0, $P < 0.05$). Grey data points are units that are not sized tuned at baseline. Stars are units that showed a significant reduction in SI ($n = 10$, $P < 0.05$). Histograms beside x and y axes show SI distribution under control and SOM hyperpolarization, respectively. The oblique histogram illustrates the distribution of changes in SI with SOM hyperpolarization. **f**, The ratio of the average response during SOM photo-hyperpolarization to the average response under control conditions plotted against stimulus size relative to peak. Same units as **d**. Inset, the same ratio without subtracting the baseline firing rate. **g**, Schematic illustration of the cortical circuit in layer 2/3 contributing to surround suppression. As a visual stimulus expands (larger stimuli are shown in lighter grey), recruitment of adjacent PCs increases SOM excitation through horizontal axons (horizontal arrows). Error bars on response ratios (**c** (inset), **f**) are estimates of s.e.m. (see Supplementary Methods for details).

inhibitory neuron, the SOM, as a key mediator of this phenomenon. This circuit is therefore likely to be involved in the contextual modulation of cortical responses to visual stimuli. The differential recruitment of pyramidal cells in superficial layers by ascending inputs and of SOMs by horizontal inputs underscores the fact that distinct neuron types are differentially integrated in the excitatory cortical circuit. These differences lead to different tuning properties, as highlighted here by the distinct size-tuning curves. Thus, although small stimuli efficiently drive layer 2/3 pyramidal cells through the activation of ascending vertical inputs, by summing activity in space via horizontal inputs, SOMs are preferentially driven by larger stimuli. As a consequence, the larger the stimulus, the stronger the SOM-mediated suppression of pyramidal cells.

An important questions is how SOMs increase their firing as a function of stimulus size if they suppress layer 2/3 pyramidal cells, that is, their main source of excitation. It is likely that the number of pyramidal cells recruited by the outer edge of the stimulus (an annulus that grows linearly with the diameter of the stimulus) more than compensate for the reduction in pyramidal-cell firing at the centre of the stimulus.

Photo-hyperpolarization of SOMs reduces but does not abolish surround suppression. Although this may partly be due to incomplete silencing of SOMs, surround suppression is probably also relayed to cortical layer 2/3 by earlier stages of visual processing[13–18], and other types of inhibitory neurons[22]or circuits[20] may also contribute to surround suppression.

The preferential recruitment of SOMs by horizontal excitatory projections is consistent with these projections having a role in size tuning[2]. In cortical layers with less extensive horizontal connectivity, size tuning may rely on different mechanisms[20,21] or may be entirely inherited from pre-cortical areas[13–18]. Importantly, because SOMs are tuned to the orientation of visual stimuli[36], they could account for the orientation dependence of surround suppression[8,9,37]. Furthermore, SOMs may respond differentially to specific stimulus properties, such as contrast, and thus also contribute to the contrast dependence of surround suppression[9,38,39]. It is likely that a connectivity pattern similar to what is described here may be present in other cortical areas as well, and thus contribute to suppressive surround in several sensory and non-sensory modalities.

METHODS SUMMARY

Experiments were performed in accordance with the regulations of the Institutional Animal Care and Use Committee of the University of California, San Diego. Mice were heterozygous for SOM-IRES-CRE (Jackson laboratory stock no. 013044) or PV-CRE (no. 008069) (except for the mice used for the experiments in Fig. 2a, b) and the reporter allele Rosa-LSL-tdTOMATO (Allen Institute line Ai9, Jackson Labs no. 007905). For Fig. 2a, b, mice were positive for Scnn1a-tg3-CRE (Jackson labs no. 009613) and crossed with the Gin (no. 003718) or B13 lines. For *in vivo* experiments, mice were implanted with a custom head plate and habituated to head fixation while running on a free-spinning circular treadmill. For targeted recording *in vivo*, tdTomato-expressing neurons were visualized by two-photon microscopy and contacted by a glass electrode containing Alexfluor 488. Extracellular unit recording was carried out using 16-channel silicon probes (Neuronexus). Single units were isolated using custom spike sorting software (Kleinfeld laboratory). We conditionally expressed ChR2 by *in utero* electroporation (for layer 2/3) or through a CRE-dependent adeno-associated virus (AAV) in Scnn1a-tg3-CRE (for layer 4). Arch or eNpHR were expressed via CRE-dependent AAVs in SOM- and PV-IRES-CRE mice. Visual stimuli were generated by custom software (Psych Toolbox) and presented on a gamma-corrected liquid crystal display monitor 15 cm from the mouse. Photostimulation *in vivo* was carried out using fibre-coupled light-emitting diodes (LEDs; Doric lenses). Photostimulation *in vitro* was carried out using a combination of fibre-coupled LEDs, or LEDs mounted and coupled to an epifluorescence microscope (Olympus BX51). eNpHR was activated by a shuttered arc lamp. Slice preparation

and intracellular recording followed previous protocols. Data acquisition, visual stimulation and statistical analysis was carried out using Igor Pro and Matlab.

Received 1 March; accepted 17 August 2012.

1. Allman, J., Miezin, F. & McGuinness, E. Direction- and velocity-specific responses from beyond the classical receptive field in the middle temporal visual area (MT). *Perception* **14,** 105–126 (1985).
2. Angelucci, A. & Bressloff, P. C. Contribution of feedforward, lateral and feedback connections to the classical receptive field center and extra-classical receptive field surround of primate V1 neurons. *Prog. Brain Res.* **154,** 93–120 (2006).
3. Gilbert, C. D., Das, A., Ito, M., Kapadia, M. & Westheimer, G. Spatial integration and cortical dynamics. *Proc. Natl Acad. Sci. USA* **93,** 615–622 (1996).
4. Hubel, D. H. & Wiesel, T. N. Receptive fields and functional architecture in two nonstriate visual areas (18 and 19) of the cat. *J. Neurophysiol.* **28,** 229–289 (1965).
5. Blakemore, C. & Tobin, E. A. Lateral inhibition between orientation detectors in the cat's visual cortex. *Exp. Brain Res.* **15,** 439–440 (1972).
6. Nelson, J. I. & Frost, B. J. Orientation-selective inhibition from beyond the classic visual receptive field. *Brain Res.* **139,** 359–365 (1978).
7. DeAngelis, G. C., Freeman, R. D. & Ohzawa, I. Length and width tuning of neurons in the cat's primary visual cortex. *J. Neurophysiol.* **71,** 347–374 (1994).
8. Knierim, J. J. & van Essen, D. C. Neuronal responses to static texture patterns in area V1 of the alert macaque monkey. *J. Neurophysiol.* **67,** 961–980 (1992).
9. Levitt, J. B. & Lund, J. S. Contrast dependence of contextual effects in primate visual cortex. *Nature* **387,** 73–76 (1997).
10. Lamme, V. A. The neurophysiology of figure-ground segregation in primary visual cortex. *J. Neurosci.* **15,** 1605–1615 (1995).
11. Dobbins, A., Zucker, S. W. & Cynader, M. S. Endstopped neurons in the visual cortex as a substrate for calculating curvature. *Nature* **329,** 438–441 (1987).
12. Mareschal, I. & Shapley, R. M. Effects of contrast and size on orientation discrimination. *Vision Res.* **44,** 57–67 (2004).
13. Solomon, S. G., Lee, B. B. & Sun, H. Suppressive surrounds and contrast gain in magnocellular-pathway retinal ganglion cells of macaque. *J. Neurosci.* **26,** 8715–8726 (2006).
14. Alitto, H. J. & Usrey, W. M. Origin and dynamics of extraclassical suppression in the lateral geniculate nucleus of the macaque monkey. *Neuron* **57,** 135–146 (2008).
15. Zhang, Y., Kim, I.-J., Sanes, J. R. & Meister, M. The most numerous ganglion cell type of the mouse retina is a selective feature detector. *Proc. Natl Acad. Sci. USA* advance online publication, doi: 10.1073/pnas.1211547109 (13 August 2012).
16. Murphy, P. C. & Sillito, A. M. Corticofugal feedback influences the generation of length tuning in the visual pathway. *Nature* **329,** 727–729 (1987).
17. Sceniak, M. P., Chatterjee, S. & Callaway, E. M. Visual spatial summation in macaque geniculocortical afferents. *J. Neurophysiol.* **96,** 3474–3484 (2006).
18. Bonin, V., Mante, V. & Carandini, M. The suppressive field of neurons in lateral geniculate nucleus. *J. Neurosci.* **25,** 10844–10856 (2005).
19. Ozeki, H. *et al.* Relationship between excitation and inhibition underlying size tuning and contextual response modulation in the cat primary visual cortex. *J. Neurosci.* **24,** 1428–1438 (2004).
20. Bolz, J. & Gilbert, C. D. Generation of end-inhibition in the visual cortex via interlaminar connections. *Nature* **320,** 362–365 (1986).
21. Ozeki, H., Finn, I. M., Schaffer, E. S., Miller, K. D. & Ferster, D. Inhibitory stabilization of the cortical network underlies visual surround suppression. *Neuron* **62,** 578–592 (2009).
22. Haider, B. *et al.* Synaptic and network mechanisms of sparse and reliable visual cortical activity during nonclassical receptive field stimulation. *Neuron* **65,** 107–121 (2010).
23. Niell, C. M. & Stryker, M. P. Highly selective receptive fields in mouse visual cortex. *J. Neurosci.* **28,** 7520–7536 (2008).
24. Van den Bergh, G., Zhang, B., Arckens, L. & Chino, Y. M. Receptive-field properties of V1 and V2 neurons in mice and macaque monkeys. *J. Comp. Neurol.* **518,** 2051–2070 (2010).
25. Margrie, T. W. *et al.* Targeted whole-cell recordings in the mammalian brain *in vivo*. *Neuron* **39,** 911–918 (2003).
26. Kawaguchi, Y. & Kubota, Y. GABAergic cell subtypes and their synaptic connections in rat frontal cortex. *Cereb. Cortex* **7,** 476–486 (1997).
27. McCormick, D. A., Connors, B. W., Lighthall, J. W. & Prince, D. A. Comparative electrophysiology of pyramidal and sparsely spiny stellate neurons of the neocortex. *J. Neurophysiol.* **54,** 782–806 (1985).
28. Taniguchi, H. *et al.* A resource of Cre driver lines for genetic targeting of GABAergic neurons in cerebral cortex. *Neuron* **71,** 995–1013 (2011); erratum **72,** 782–806 (2011).
29. Boyden, E. S., Zhang, F., Bamberg, E., Nagel, G. & Deisseroth, K. Millisecond-timescale, genetically targeted optical control of neural activity. *Nature Neurosci.* **8,** 1263–1268 (2005).
30. Petreanu, L., Mao, T., Sternson, S. M. & Svoboda, K. The subcellular organization of neocortical excitatory connections. *Nature* **457,** 1142–1145 (2009).
31. Adesnik, H. & Scanziani, M. Lateral competition for cortical space by layer-specific horizontal circuits. *Nature* **464,** 1155–1160 (2010).
32. Wang, Q. & Burkhalter, A. Area map of mouse visual cortex. *J. Comp. Neurol.* **502,** 339–357 (2007).
33. Kapfer, C., Glickfeld, L. L., Atallah, B. V. & Scanziani, M. Supralinear increase of recurrent inhibition during sparse activity in the somatosensory cortex. *Nature Neurosci.* **10,** 743–753 (2007).
34. Chow, B. Y. *et al.* High-performance genetically targetable optical neural silencing by light-driven proton pumps. *Nature* **463,** 98–102 (2010).
35. Atasoy, D., Aponte, Y., Su, H. H. & Sternson, S. M. A. FLEX switch targets Channelrhodopsin-2 to multiple cell types for imaging and long-range circuit mapping. *J. Neurosci.* **28,** 7025–7030 (2008).
36. Ma, W. P. *et al.* Visual representations by cortical somatostatin inhibitory neurons–selective but with weak and delayed responses. *J. Neurosci.* **30,** 14371–14379 (2010).
37. Cavanaugh, J. R., Bair, W. & Movshon, J. A. Selectivity and spatial distribution of signals from the receptive field surround in macaque V1 neurons. *J. Neurophysiol.* **88,** 2547–2556 (2002).
38. Kapadia, M. K., Westheimer, G. & Gilbert, C. D. Dynamics of spatial summation in primary visual cortex of alert monkeys. *Proc. Natl Acad. Sci. USA* **96,** 12073–12078 (1999).
39. Sceniak, M. P., Ringach, D. L., Hawken, M. J. & Shapley, R. Contrast's effect on spatial summation by macaque V1 neurons. *Nature Neurosci.* **2,** 733–739 (1999).

Supplementary Information is available in the online version of the paper.

Acknowledgements We are grateful to J. Evora for the reconstruction of SOMs and technical assistance. We thank C. Niell and M. Stryker for providing expertise and sharing code used at the initial stages of this project; S. Olsen for providing the firing rates of part of the units isolated under anaesthesia; P. Abelkop and A. Linder for technical assistance; and J. Isaacson and members of the Scanziani laboratory for helpful advice. H.A. was supported by the Helen Hay Whitney Foundation and the Howard Hughes Medical Institute (HHMI). W.B. and M.S. were supported by the HHMI, the Gatsby charitable foundation and US National Institute of Health grant NS069010.

Author Contributions H.A. and M.S. designed the study. H.A. conducted all experiments. W.B. conducted all *in vivo* data analysis and spike sorting. H.T. and Z.J.H. generated the SOM-IRES-CRE mice. M.S. and H.A. wrote the paper.

Author Information Reprints and permissions information is available at www.nature.com/reprints. The authors declare no competing financial interests. Readers are welcome to comment on the online version of the paper. Correspondence and requests for materials should be addressed to M.S. (massimo@ucsd.edu).